Combustion and Flame 257 (2023) 112311

Contents lists available at ScienceDirect

Combustion and Flame

journal homepage: www.elsevier.com/locate/combustflame

The $NH_3/NO_2/O_2$ system: Constraining key steps in ammonia ignition and N_2O formation

Peter Glarborg

DTU Chemical Engineering, Technical University of Denmark, LyngbyDK-2800, Denmark

ARTICLE INFO

Article history:
Received 20 April 2022
Revised 17 July 2022
Accepted 20 July 2022
Available online 6 August 2022

Keywords:
NH3
NO2
N2O
Chemical kinetics
Flow reactor experiments

ABSTRACT

Amine/NO_2 interactions are important for ignition and N_2O emissions in ammonia combustion. In the present work, reported results from batch reactors (580–690 K) and flow reactors (850–1350 K) for the NH_3/NO_2 system were re-interpreted in terms of the present understanding of the amine chemistry. Furthermore, additional flow reactor results on the impact of O_2 on the NH_3/NO_2 reaction were presented and analyzed. Based on the experimental results and the modeling analysis, it was possible to constrain the rate constants for reactions of NH_3 and NH_2 with NO_2 and for subsequent steps involving H_2NO and HNO intermediates. The key reaction is $NH_2 + NO_2$, forming $H_2NO + NO$ (R2) and $N_2O + H_2O$ (R3). The results indicate that the yield of N_2O in the $NH_2 + NO_2$ reaction decreases with temperature in the 850–1350 K range, in agreement with the theoretical study by Klippenstein and coworkers. The fate of H_2NO and HNO is important for the overall reactivity. In the absence of O_2, formation of chain carriers is controlled by the sequence $H_2NO + NO_2 \rightarrow HNO + HONO$, $HNO + NO_2 \rightarrow NO + HONO$, $HONO (+M) \rightarrow NO + OH (+M)$. At higher temperatures, in the presence of O_2, the sequence $H_2NO + O_2 \rightarrow HNO + HO_2$, $HNO + O_2 \rightarrow NO + HO_2$, $NO + HO_2 \rightarrow NO_2 + OH$ enhances radical formation and recycles NO_2. The satisfactory agreement between experiments and modeling predictions, both without and with O_2, supports the present rate constants for the reactions of H_2NO and HNO with NO_2 and O_2, respectively.

1. Introduction

Ammonia is of interest as a carbon-free fuel and challenges of using ammonia in engines and gas turbines are investigated extensively [1–3]. These include poor ignition and combustion properties, as well as the formation of the strong greenhouse gas N_2O. To address these issues, it is important to develop reliable kinetic models for ignition and oxidation of ammonia. Several kinetic models for ammonia oxidation have been published in recent years, including those of Mathieu and Petersen [4], Li et al. [5], Otomo et al. [6], Glarborg et al. [7], Mei et al. [8,9], Stagni et al. [10], and Jiang et al. [11]. A number of these models were tested by Valera-Medina et al. [3] who showed that none of the mechanisms provided accurate predictions over a wide range of conditions.

In diesel engines, the ignition of ammonia takes place at intermediate temperatures and high pressure. These conditions have been approximated in a number of rapid compression machine (RCM) experiments [12–14]. The results confirm the poor ignition properties of ammonia, but also point to deficiencies of kinetic models in predicting the observed behavior. The conditions prior to ignition in engines involve aspects of the amine chemistry that are not well established at present. Formation of HO_2 through $H + O_2$ (+M) recombination is enhanced by the high pressure and HO_2 becomes the dominating radical. The peroxide may also be formed by H-abstraction reactions involving O_2, primarily with H_2NO and HNO [15]. The reaction of HO_2 with NH_2 is now known to form predominantly $NH_3 + O_2$ [10,16–18]. This step is chain-terminating and in current models, it leads to overprediction of ignition delays at elevated pressure [18]. However, in the presence of NO, HO_2 promotes formation of NO_2 in the fast reaction [7],

$$NO + HO_2 \rightleftarrows NO_2 + OH \quad \text{(R17)}$$

The reaction numbers correspond to Table 1 below. Miller and coworkers were among the first to recognize the importance of NO_2 in NH_3 oxidation, selective non-catalytic reduction (SNCR) of NO by NH_3, and formation of N_2O, and they studied this chemistry in a sequence of publications [7,19–22].

Two aspects of the chemistry involving NO_2 are of particular interest. The first is the role of NO_2 in ignition. Nitric oxide, formed as part of the pre-ignition chemistry, will be partly converted to NO_2 by the fast reaction with HO_2 (R17). The OH radical

E-mail address: pgl@kt.dtu.dk

https://doi.org/10.1016/j.combustflame.2022.112311

Table 1
Selected reactions in the $NH_3/NO_2/O_2$ reaction subset. Parameters for use in the modified Arrhenius expression $k=AT^{\beta}\exp(-E/[RT])$. Units are mol, cm, s, cal.

		A	β	E	Source
1.	$NH_2 + HONO \rightleftarrows NH_3 + NO_2$	6.4E03	2.340	-3200	See text
2.	$NH_2 + NO_2 \rightleftarrows H_2NO + NO$	1.1E12	0.110	-1186	See text
		-4.3E17	-1.874	588	*a*
3.	$NH_2 + NO_2 \rightleftarrows N_2O + H_2O$	4.3E17	-1.874	588	See text
4.	$NH_2 + NO \rightleftarrows N_2 + H_2O$	2.6E19	-2.369	870	[33]
5.	$NH_2 + NO \rightleftarrows NNH + OH$	4.3E10	0.294	-866	[33]
6.	$NO + OH(+M) \rightleftarrows HONO(+M)$	1.1E14	-0.300	0	[34]
	Low pressure limit (He)	3.4E23	-2.500	0	
	Troe parameters: 0.75 1E-30 1E30 1E30				
	Collision efficiencies Ar=1.1, N_2=2, NH_3=4				
7.	$HONO + OH \rightleftarrows NO_2 + H_2O$	1.7E12	0.000	-520	[35]
8.	$HNO + H(+M) \rightleftarrows H_2NO(+M)$	5.5E13	0.000	3250	[36]
	Low pressure limit	1.5E19	-1.632	0	[37] (rv)
9.	$H_2NO + OH \rightleftarrows HNO + H_2O$	2.1E15	-0.751	-464	[17]
10.	$H_2NO + O_2 \rightleftarrows HNO + HO_2$	2.3E02	2.994	18,900	[15]
11.	$H_2NO + NH_2 \rightleftarrows NH_3 + HNO$	1.8E06	1.940	-580	[37]
12.	$H_2NO + NO_2 \rightleftarrows HNO + HONO$	8.0E11	0.000	6000	See text
13.	$NO + H(+M) \rightleftarrows HNO(+M)$	1.5E15	-0.410	0	[38]
	Low pressure limit	2.4E14	0.206	-1550	[39]
	Troe parameters: 0.82 1E-30 1E30 1E30				
	Collision efficiencies N_2=1.6, NH_3=4				
14.	$HNO + O_2 \rightleftarrows NO + HO_2$	4.0E05	2.300	14,605	[40]
15.	$HNO + NH_2 \rightleftarrows NH_3 + NO$	5.9E02	2.950	-3469	[41]
16.	$HNO + NO_2 \rightleftarrows NO + HONO$	7.9E02	3.060	3882	[42]
17.	$NO + HO_2 \rightleftarrows NO_2 + OH$	2.1E12	0.000	-497	[43]
18.	$NO_2 + H \rightleftarrows NO + OH$	1.3E14	0.000	362	[7]
19.	$NNH \rightleftarrows N_2 + H$	1.0E09	0.000	0	[7]

a: duplicate reaction - the resulting rate constant is calculated as the sum of the two expressions.

will mainly react with NH_3, $NH_3 + OH \rightleftarrows NH_2 + H_2O$. The $NH_2 + NO_2$ reaction can then initiate a sequence of reactions that promotes further NO_2 formation,

$$NH_2 + NO_2 \rightleftarrows H_2NO + NO$$

$$H_2NO + O_2 \rightleftarrows HNO + HO_2 \quad (R10)$$

$$HNO + O_2 \rightleftarrows NO + HO_2 \quad (R14)$$

This sequence of reactions, including regeneration of NO_2 in R17, corresponds to the overall, chain-branching reaction $NH_3 + 2O_2 \rightarrow NO_2 + H_2O + OH$, which promotes ignition. Reactions of NO_2 are also part of another chain-branching sequence,

$$H_2NO + NO_2 \rightleftarrows HNO + HONO \quad (R12)$$

$$HNO + NO_2 \rightleftarrows NO + HONO \quad (R16)$$

$$HONO(+M) \rightleftarrows NO + OH(+M) \quad (R6b)$$

This sequence disrupts the NO_2 recycling, but promotes formation of chain carriers since HONO dissociates easily. Predicted ignition delays under RCM conditions are sensitive to these reactions [14], which generally are not well characterized.

The second interesting aspect of NO_2 is its role in the formation of N_2O. Interaction of amine radicals with nitrogen oxides offers two routes to N_2O,

$$NH + NO \rightleftarrows N_2O + H$$

$$NH_2 + NO_2 \rightleftarrows N_2O + H_2O \quad (R3)$$

At higher temperatures, N_2O is formed mainly by the NH + NO reaction, while at lower temperatures, $NH_2 + NO_2$ is the main source. The high temperature formation is not a large concern, because under these conditions N_2O has a short lifetime; it is rapidly consumed by thermal dissociation or reaction with atomic H,

$$N_2O(+M) \rightleftarrows N_2 + O(+M)$$

$$N_2O + H \rightleftarrows N_2 + OH$$

In terms of emission from engines, the main issue is the N_2O formation at the lower temperatures at the end of a cycle. Here, unburned NH_3, possibly released from crevices, may react to form N_2O in reaction R3. Even though this product channel is secondary compared to R2, it may still constitute a significant source of N_2O. With decreasing temperature, the probability of *in-situ* reduction of N_2O decreases significantly.

Despite the importance of amine/NO_2 interactions for ignition and greenhouse gas emissions in ammonia combustion, this chemistry is not well established. Both reactions of amines with NO_2 and subsequent steps involving HONO, H_2NO, and HNO intermediates are uncertain. The objective of the present work is analyze the NH_3/NO_2 reaction system to identify constraints on the kinetic model and thereby facilitate more accurate predictions of ignition delays for NH_3 and formation of N_2O. Glarborg et al. [19] investigated the NH_3/NO_2 system in a flow reactor with the aim to characterize the rate constant and product branching ratio for the $NH_2 + NO_2$ reaction. In addition, results for the NH_3/NO_2 system have been reported from batch reactor experiments [23–25] in studies of the direct reaction of NH_3 with NO_2,

$$NH_3 + NO_2 \rightleftarrows NH_2 + HONO \quad (R1b)$$

In the present work, the batch and flow reactor data are reinterpreted in terms of the present understanding of the amine chemistry. Furthermore, novel flow reactor results on the impact of O_2 on the NH_3/NO_2 reaction are presented and analyzed.

2. Experimental

A detailed description of the flow reactor and the experimental procedures is available elsewhere [26], and only a brief description is given here. A quartz flow reactor designed for obtaining plug flow in the laminar flow regime was placed in a three–zone electrically heated oven, securing a uniform temperature profile within ±7 K in the isothermal zone. The reactor temperature was measured by a thermocouple placed in a quartz tube with no access for the reactant gases. The gaseous components were led to the quartz reactor in as many as four separate streams. The main flow contained nitrogen while the reactants were supplied through separate injector tubes. In order to achieve a well defined reactor volume, the main flow and the injector flows were heated separately and mixed in cross flow at the reactor inlet. The reactor tube used in the present experiments had a diameter of 0.9 cm. The product gas was quenched at the outlet of the reactor tube, but kept heated at 453 K downstream to avoid adsorption of NH_3 on the walls prior to the gas analyzers. Adsorption of ammonia in the inlet system and the reactor itself is not an issue because the experiments are conducted under stationary conditions allowing surfaces to be saturated.

Nitric oxide (NO) was measured by Hartman & Braun gas analyzer Radas 1G (UV resonance absorption). Nitrous oxide (N_2O) was measured by Perkin Elmer analyzer Spectran 647 utilizing an NDIR-photometric technique. The analyzers were calibrated using standard gas mixtures before use; the measured values are valid within ±3%, with an uncertainty of at least ±10 ppmv. The N_2O analyzer was cross-sensitive to NH_3 and measurements were corrected to account for this cross-sensitivity. Concentrations of NH_3 and NO_2 were measured with Opsis analyzer AR 600, utilizing the ultraviolet–visible wavelength range. For these species we estimate an uncertainty of ±20%, but not less than ±20 ppm. All experiments were conducted at very dilute conditions to avoid significant heat generation.

3. Detailed chemical kinetic model

The chemical kinetic model, including rate coefficients and thermodynamic data, was drawn mainly from the review of nitrogen chemistry by Glarborg et al. [7], but with modifications based on more recent work and the present analysis. The H_2-O_2 subset [27,28] was updated according to the work by Burke and Klippenstein on chemically termolecular reactions H + O_2 + R [29] and by Klippenstein et al. [30] on HO_2 + HO_2. The amine subset was revised based on work on a number of reactions, including NH_2 + H (+M) [16,31], NH_3 + HO_2 [10], NH_2 + HO_2 [16,17], and steps in the diazene subset [32]. Table 1 lists selected reactions from the NH_3/NO_2/O_2 reaction subset.

The key reactions include NH_3 + NO_2 (R1b) and NH_2 + NO_2 (R2,R3). Figure 1 shows an Arrhenius plot of the NH_2 + HONO reaction,

$$NH_2 + HONO \rightleftarrows NH_3 + NO_2 \quad (R1)$$

The experimental data from Rosser and Wise [23] and Bedford and Thomas [24] are shown as the apparent rate constants, which are strongly affected by secondary reactions. In the present work, selected experimental results from Bedford and Thomas were reinterpreted to obtain a more accurate rate constant for R1. Based on the analysis, discussed in detail below, a value of $k_1(619\ K) = 3.0{\cdot}10^{11}$ cm^3 mol^{-1} s^{-1} was obtained. This value agrees within 30% with the theoretical rate constant from Xu and Lin [44]. We have adjusted slightly the pre-exponential factor in their expression to match the data point at 619 K (see Table 1).

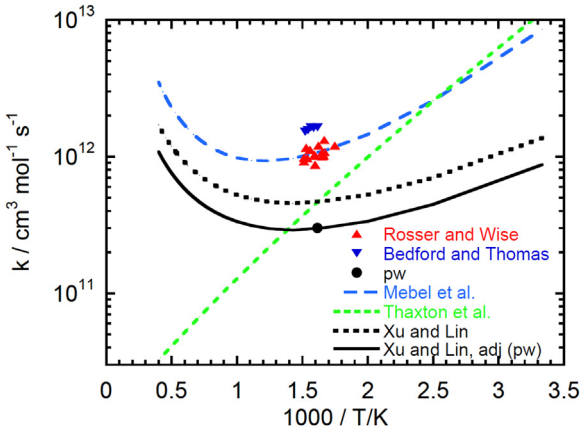

Fig. 1. Arrhenius plot for the reaction NH_2 + HONO → NH_3 + NO_2 (R1). The symbols denote the measured values, i.e., the apparent rate constants by Rosser and Wise [23] and Bedford and Thomas [24] (both reversed from k_{1b} through the equilibrium constant), and the value derived in the present work from reinterpretation of the Bedford and Thomas data at 619 K. The lines denote the rate constants derived from kinetic modeling of earlier experiments [23,24] by Thaxton et al. [45], calculated from theory by Mebel et al. [46] and Xu and Lin [44], and the value preferred in the current work.

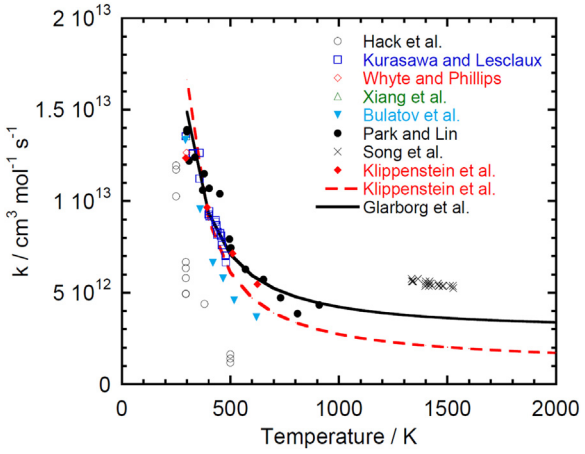

Fig. 2. Arrhenius plot for the reaction NH_2 + NO_2 → products. The symbols denote measurements of the rate constant, drawn from Hack et al. [47], Kurasawa and Lesclaux [48], Whyte and Phillips [49], Xiang et al. [50], Bulatov et al. [51], Park and Lin [54], Song et al. [55], and Klippenstein et al. [56]. The dashed line denotes the theoretical value by Klippenstein et al. [56], while the solid line denotes the recommendation by Glarborg et al. [7].

The NH_2 + NO_2 reaction has been studied over a wide range of temperature. It has two major product channels,

$$NH_2 + NO_2 \rightleftarrows H_2NO + NO \quad (R2)$$

$$NH_2 + NO_2 \rightleftarrows N_2O + H_2O \quad (R3)$$

Values for the overall rate constant [19,47–56] show significant scatter (Fig. 2), but most recent determinations below 1000 K are in reasonable agreement. The rate constant calculated by Klippenstein et al. [56] provides a good description these data, but it is a factor of three below the shock tube determination of Song et al. [55] at 1300–1600 K. In the present work, we have adopted the overall rate constant from Glarborg et al. [7], which is compatible with the values from both Song et al. and Klippenstein et al. within their uncertainties.

Also the branching fraction for the NH_2 + NO_2 reaction, defined as $\beta = k_3/(k_2 + k_3)$, has been in discussion. Figure 3 compares measured and theoretical values. A high value of 0.59 at

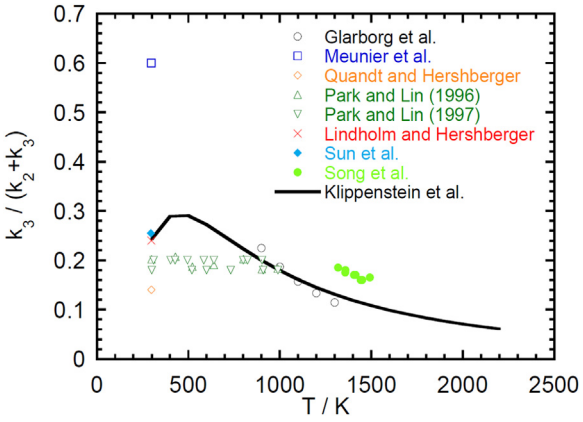

Fig. 3. Branching ratio, defined as $\beta = k_3/(k_2 + k_3)$, for the reaction $NH_2 + NO_2 \rightarrow$ products. The symbols denote measured values, drawn from Glarborg et al. [19], Meunier et al. [53], Quandt and Hershberger [57], Park and Lin [54,58], Lindholm and Hershberger [59], Sun et al. [60], and Song et al. [55]. The solid line denotes the value calculated by Klippenstein et al. [56].

room temperature was reported by Meunier et al. [53], but most experimental data at low temperature support a value of 0.2±0.05 [54,57–60]. At higher temperatures, the experimental work of Park and Lin [54,58] indicates a branching fraction of 0.2, independent of temperature; this is supported by a recent theoretical study of Cui et al. [61]. However, the flow reactor results analyzed in the present work and the shock tube study of Song et al. [55] indicate a value that decreases slightly with temperature. This behavior is captured in the theoretical study by Klippenstein et al. [56]. We have combined the calculated value of $\beta = 3.9{\cdot}10^5\ T^{-1.984}\ \exp(-893/T)$ from Klippenstein et al. with the overall rate constant from the review of Glarborg et al. [7] to obtain the values of k_2 and k_3 listed in Table 1.

The fate of the oxygenated intermediates formed in reactions R1 and R2, HONO and H_2NO, has a significant impact on the reaction rate and final products. Nitrous acid, HONO, which can also be formed by H-abstraction reactions involving NO_2, is consumed by thermal dissociation (R6b) or by reaction with OH (R7) under the current conditions. There are no experimental data for the dissociation, but the reverse step,

$$NO + OH(+M) \rightleftarrows HONO(+M) \qquad (R6)$$

has been studied at low temperature over a wide range of pressure. The rate constant derived by Fulle et al. [34] is in good agreement with the recent re-evaluation by Chen et al. [62]. The low-pressure limit reported by Fulle et al. was obtained for He as bath gas. Helium has a collision efficiency slightly lower than Ar [63]; the value for N_2 compared to Ar has been reported to be in the range 1.7–2.1 [63–67]. Based on analogy with amine reactions [16], the NH_3 collision efficiency can be expected to be significantly higher. For the reaction of HONO with OH, we adopt the rate constant measured at low temperature by Burkholder et al. [35]; the value extrapolates well to the high temperature results of Fifer [68].

The H_2NO/HNO subset of the mechanism involves significant uncertainties. For dissociation of H_2NO (R8b), we rely on the estimate of Dean and Bozzelli [37] for the low-pressure limit. We have converted it to the reverse step (R8) through the equilibrium constant and combined it with the calculated high-pressure limit from Page and Soto [36]. The measurements by Sun et al. [60] indicate that the H_2NO + OH reaction (R9) is extremely fast at room temperature, but the recent theoretical study by Klippenstein and Glarborg [17] shows a significant negative temperature dependency.

Under the conditions of the present study, H_2NO reacts primarily with NO_2 (R12) or, if present, O_2 (R10). There are no measurements of the $H_2NO + NO_2$ reaction, but Sun et al. [60] were not able to detect reaction between the two species at room temperature. The present analysis allows us to put further constraints of the value of k_{12}. The batch reactor results of Park and Lin [25] can only be explained in terms of a value for k_{12} that is sufficiently high to make it the main consumption channel for H_2NO in the 580–690 K range (see discussion below). However, due the sensitivity to other steps, it is not possible to derive a lower limit for k_{12} from these data. The flow reactor results for NH_3/NO_2 [19], with the constraints imposed on other reactions, allow us to estimate a value of $k_{12} \approx 5{\cdot}10^{10}$ cm^3 mol^{-1} s^{-1} at 1000 K. Assuming an activation energy of 6 kcal mol^{-1} similar to the barrier calculated for the HNO + NO_2 reaction (R16) [69], we arrive at the rate constant listed in Table 1. For $H_2NO + O_2$, we have adopted the rate constant calculated by Song et al. [15]; it is somewhat slower than the recent theoretical value from Chavario Canas et al. [70].

An alternative consumption channel for H_2NO is the isomerization to HNOH, followed by reaction of HNOH mainly with NO_2 to form HNO and HONO. Even though HNOH is about 8 kcal mol^{-1} higher in energy than H_2NO, we tentatively assume that its reactions with NO_2 and other stable species have rate constants similar to those of H_2NO.

The most important reactions of HNO include thermal dissociation (R13b) and H-abstraction by NH_2 (R15), NO_2 (R16), and O_2 (R14). Recombination of H with NO (R13) has been measured from room temperature up to 900 K by Riley et al. [39] and derived theoretically by Stagni et al. [10]. Both expressions agree well with flow reactor measurements at 1000–1200 K by Allen et al. [71] and Glarborg et al. [72], but exhibit different temperature dependencies. For now, we have adopted the recommendation of Riley et al., but more work is desirable on this step. The same is true for reactions R14-R16 for which no experimental data are available. The rate constant for HNO + O_2 (R14) was estimated by Dean and Bozzelli [37] by QRRK methods and calculated more recently at a higher level of theory by Wang et al. [40]. For HNO + NO_2 (R16), theoretical studies have been reported by Mebel et al. [69] and Shang et al. [42]. For both steps we adopt the more recent evaluation.

4. Results and discussion

A major objective of the present work is to put constraints on the kinetic model to improve its accuracy in predicting ignition delays for NH_3 and formation of N_2O. Results for the NH_3/NO_2 system have been reported in literature from batch reactor [23–25] and flow reactor [19] experiments. Below, these data are re-interpreted in terms of the present understanding of the amine chemistry. Furthermore, novel flow reactor results on the impact of O_2 on the NH_3/NO_2 reaction are presented and analyzed.

4.1. Batch reactor results

The experiments of Rosser and Wise [23] and Bedford and Thomas [24] were conducted in batch reactors at temperatures between 580 and 800 K. The reactant mixtures were undiluted, with NH_3 in large excess compared to NO_2. In both studies, the authors, monitoring the NO_2 concentration, found that the reaction rate decreased over time. Bedford and Thomas correctly attributed this to the formation of NO, followed by the chain terminating step NH_2 + NO → N_2 + H_2O (R4), which at these temperatures dominates over the propagating channel to NNH + OH (R5).

Re-interpretation of the experiments of Bedford and Thomas [24] allows us to obtain a more reliable rate constant for the $NH_3 + NO_2$ reaction (R1b). At a temperature of 619 K, Bedford and Thomas investigated the effect of adding various amounts of NO. Under conditions, where NO is in large

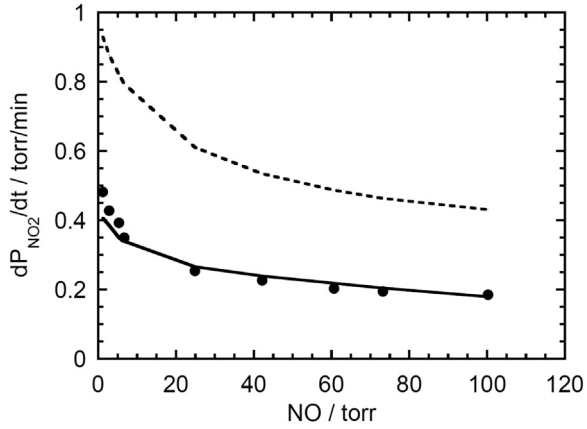

Fig. 4. Comparison of experimental data at 619 K from Bedford and Thomas [24] with modeling predictions for the initial NO_2 consumption rate as a function of NO addition in the reaction of NH_3/NO_2 mixtures in a low pressure batch reactor. Symbols denote experimental data, while the solid line denotes modeling predictions with the present mechanism, including a rate constant $k_1(619\ K) = 3.0{\cdot}10^{11}$ $cm^3\ mol^{-1}\ s^{-1}$. The dashed line denotes predictions with the rate constant derived by Bedford and Thomas. Starting conditions: 44 torr NH_3 and 6.1 torr NO_2; varying NO.

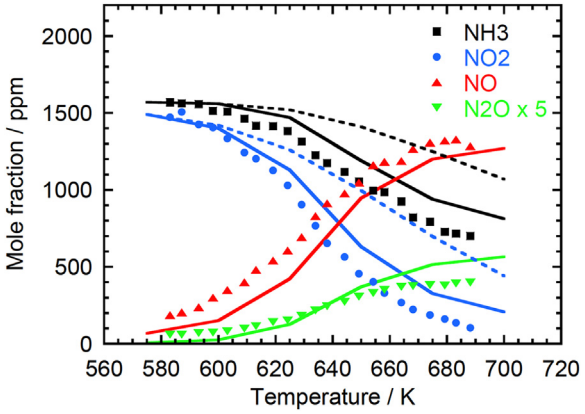

Fig. 5. Comparison of experimental data of Park and Lin [25] and modeling predictions for species mole fractions in the reaction of an NH_3/NO_2 mixture in an atmospheric pressure batch reactor. Symbols denote experimental data, while solid lines denote modeling predictions with the present model. The dashed lines show the effect of setting $k_{12} = 0$. Conditions: NH_3 = 1580 ppm, NO_2 = 1570 ppm (balance Ar); residence time 2400 s.

excess over NO_2, NH_2 formed in R1b reacts almost exclusively with NO. At 619 K, the NH_2 + NO reaction leads predominantly (almost 85%) to N_2 + H_2O (R4). A small fraction of the NH_2 + NO reaction forms NNH + OH (R5), initiating the sequence $NH_2 + NO \rightarrow NNH + OH$ (R5), $NNH \rightarrow N_2 + H$ (R19), $NO_2 + H \rightarrow NO + OH$ (R18), $NO + OH(+M) \rightarrow HONO(+M)$ (R6). The OH formed in reactions R5 and R18 reacts almost exclusively with NO to form HONO, which is stable due to the large excess of NO. The secondary chemistry is thus very limited and can be taken accurately into account. This means that the value of k_1 can be derived with an uncertainty largely limited to experimental error. From the data obtained at high NO levels, we derive a value of $k_1(619\ K) = 3.0{\cdot}10^{11}$ $cm^3\ mol^{-1}\ s^{-1}$.

Figure 4 shows a comparison between the results of Bedford and Thomas for dP_{NO2}/dt at 619 K and modeling predictions as a function of the NO partial pressure. At NO levels above 20 torr, the NO_2 consumption rate is almost constant, in line with the discussion above. Below 20 torr, dP_{NO2}/dt increases with decreasing NO addition. At low levels of NO, the NH_2 + NO_2 reaction dominates over NH_2 + NO, forming mostly H_2NO + NO (R2). Under these conditions, the consumption rate of NO_2 depends strongly on the secondary reactions of H_2NO and HNO, which both may react with NO_2 (R12, R16), promoting reaction. The model captures well the experimental results.

Park and Lin [25] reported mole fractions of NH_3, NO_2, NO, and N_2O in the reaction of a very dilute NH_3/NO_2 mixture in a batch reactor. The experiments were conducted at 580–690 K and atmospheric pressure at long reaction times (2400 s). Figure 5 shows a comparison between their measurements and modeling predictions. Ammonia and nitrogen dioxide concentrations decrease monotonically with increasing temperature, with the NO_2 consumption rate roughly two times faster than that of NH_3. The main product detected is NO, with lower levels of N_2O.

The present model provides a good description of the observed behavior. The reaction sequence responsible for enhancing the NO_2 consumption rate is NH_2 + $NO_2 \rightarrow H_2NO$ + NO (R2), H_2NO+$NO_2 \rightarrow$ HNO + HONO (R12), HNO + $NO_2 \rightarrow$ NO + HONO (R16), followed by partial thermal dissociation of HONO (R6b). The reaction NO_2 + $NO_2 \rightarrow$ NO + NO + O_2 also consumes NO_2, in effect acting as a chain-terminating step. The predicted consumption rates of the reactants are sensitive to the fate of H_2NO. If its reaction with NO_2 to form HONO and NO (R12) is too slow to be competitive, the overall reaction rate is strongly reduced. The dashed lines show predictions for NH_3 and NO_2 for $k_{12} = 0$. Due to the impact of side reactions, it is not possible to derive a lower limit for k_{12}. However, to show up as sensitive in the calculations, k_{12} would need to be around or lower than 10^8 $cm^3\ mol^{-1}\ s^{-1}$ at 650 K; well below the current estimate.

4.2. Flow reactor results

As described above, flow reactor experiments of NH_3/NO_2 mixtures without [19] and with (present work) O_2 addition were conducted in a laminar flow quartz reactor. The temperature range covered was 850–1350 K. The inlet composition was roughly 500 ppm NH_3, 285 or 500 ppm NO_2, and 0 or 2% O_2. Table 2 summarizes the experimental conditions.

Ammonia is sensitive to surfaces and it is known that heterogeneous reactions on the quartz reactor wall may serve to shorten the induction time in laminar flow reactors [7,73]. The $NH_3/NO/O_2$ system (SNCR) is not sensitive to initiation, but calculations for mixtures of NH_3/NO_2 and $NH_3/NO_2/O_2$ show significant induction times and the results may thus be affected by surface initiation. This phenomenon is not important for the batch reactor results discussed above. The data of Bedford and Thomas [24] (Fig. 4) were obtained as a gradient dNO_2/dt after onset of reaction and can be assumed to be independent of the initiation conditions [74]. For the experiments of Park and Lin [25] (Fig. 5), the initiation time was small compared to the long total residence time, and calculations were not sensitive to initiation.

The mechanism of surface initiation is not known, but conceivably it involves a partial oxidation of NH_3 on an active site, followed by desorption of the product to the gas phase. To account for this phenomena in the modeling, we introduce 1 ppm of HONO in the inlet composition. This serves to shorten the predicted induction time below 1000 K, while the impact is small at higher temperatures.

Figures 6–9 show comparisons between the measured and predicted mole fractions of NH_3, NO_2, NO, and N_2O. The observed behavior for the NH_3/NO_2 mixtures is similar to that observed for batch reactor experiments at lower temperatures and longer residence times by Park and Lin [25] (Fig. 5). The NH_3 and NO_2 concentrations decrease with increasing temperature, with NO_2 consumed more rapidly than NH_3. Nitric oxide is the major detected product, with nitrous oxide also formed.

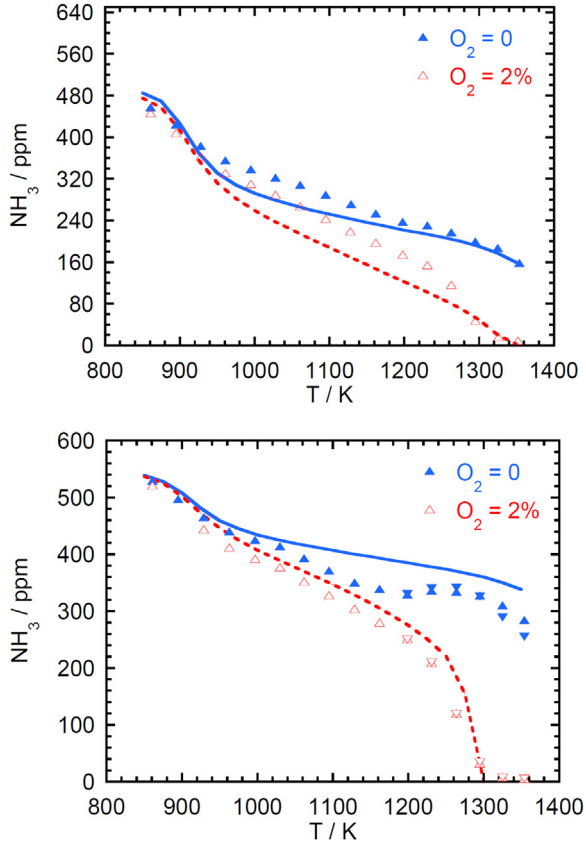

Fig. 6. Comparison of experimental data and modeling predictions for the NH_3 mole fractions in reaction of NH_3/NO_2 mixtures without [19] and with (pw) addition of O_2 in an atmospheric pressure flow reactor. Symbols denote experimental data, while lines denote modeling predictions. Upper figure: NH_3 = 492/483 ppm, NO_2 = 515/505 ppm, NO = 55/55 ppm, O_2 = trace/2.0%. Lower figure: NH_3 = 547/535 ppm, NO_2 = 285/273 ppm, NO = 32/32 ppm, O_2 = trace/2.1%. Carrier gas N_2, residence time (s) ≈ 107/T(K), pressure 1.09 atm. Conditions for repeated experiments are listed in Table 2.

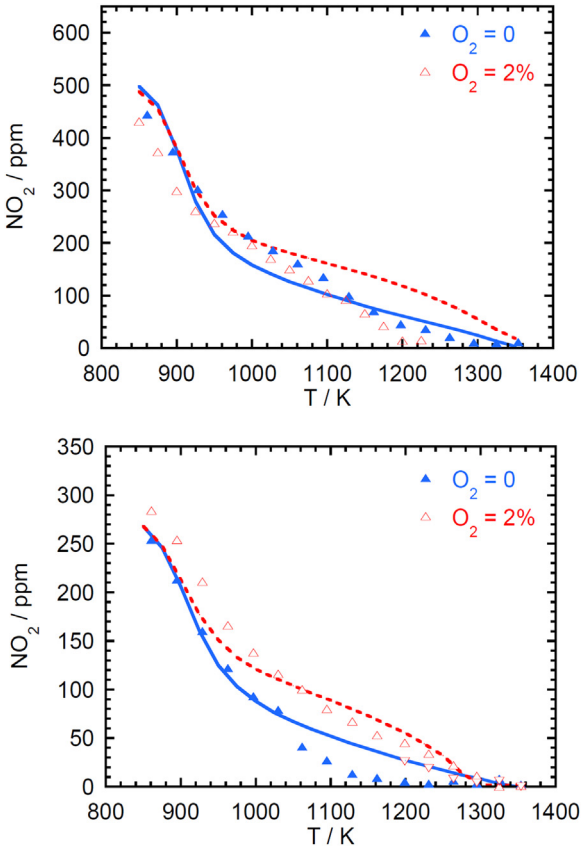

Fig. 7. Comparison of experimental data and modeling predictions for the NO_2 mole fractions in reaction of NH_3/NO_2 mixtures without [19] and with (pw) addition of O_2 in an atmospheric pressure flow reactor. Symbols denote experimental data, while lines denote modeling predictions. Upper figure: NH_3 = 492/483 ppm, NO_2 = 515/505 ppm, NO = 55/55 ppm, O_2 = trace/2.0%. Lower figure: NH_3 = 547/535 ppm, NO_2 = 285/273 ppm, NO = 32/32 ppm, O_2 = trace/2.1%. Carrier gas N_2, residence time (s) ≈ 107/T(K), pressure 1.09 atm. Conditions for repeated experiments are listed in Table 2.

Table 2
Experimental conditions. τ is the residence time in the isothermal zone and P is the pressure.

	NH_3 (ppm)	NO_2 (ppm)	NO (ppm)	O_2 (%)	τ (s)	P (atm)	Source
1.	492	515	55	trace	107/T(K)	1.09	[19]
2.	483	505	55	2.0%	104/T(K)	1.09	pw
3.	547	285	32	trace	110/T(K)	1.09	[19]
	543	279	32	trace	106/T(K)	1.09	
4.	535	273	32	2.1%	108/T(K)	1.09	pw
	532	273	32	2.1%	103/T(K)	1.09	

The presence of O_2 enhances the NH_3 consumption, most pronounced at temperatures above 1250 K and at the higher NH_3/NO_2 inlet ratio. Contrary to this, the NO_2 consumption is either unaffected (at 500 ppm NO_2, Fig. 7a) or slightly inhibited (285 ppm NO_2, Fig. 7b). The NO formation is inhibited in the presence of O_2 above 1000 K, whereas N_2O is promoted.

The modeling predictions are generally in satisfactory agreement with the experiments and may help to explain the observed trends. However, there are some noteworthy discrepancies, in particular the underprediction of NO above 1100 K in the absence of O_2 and the overprediction of N_2O above 1150 K in the presence of O_2.

In the presence of O_2, the NO_2 recycle loop, involving R2, R12, R16, R6b, and R17, leads to a higher NO_2 availability. Under these conditions, NO_2 is regenerated by the reaction NO + HO_2 → NO_2 + OH. The higher NO_2 concentration in turn leads to an increased formation of N_2O, compared to experiments conducted without addition of O_2. This phenomena is observed both experimentally and in modeling. However, under oxidizing conditions the N_2O yield is overpredicted at temperatures above 1100 K, indicating that the balance in the model for H_2NO and HNO reacting with NO_2 or O_2, respectively, is not captured accurately.

Figure 10 shows a reaction path diagram for conversion of NH_3 in the presence of NO_2, without and with O_2 present. The reaction NH_3 + NO_2 (R1b) is an important initiation step and at lower temperatures (around 650 K), where the O/H radical pool develops slowly, it remains significant for consumption of NH_3. At elevated temperature, where OH is formed in significant amounts from dissociation of HONO (R6b), NH_3 is consumed almost solely by reaction with OH. The NH_2 radical reacts mostly with NO_2 (R2, R3), even though NH_2 + NO (R4, R5) becomes more competitive as the nitric oxide concentration increases. The NH_2 + NO_2 reaction yields mostly H_2NO + NO (R2). In the absence of O_2, H_xNO (H_2NO and HNO) reacts mainly with NO_2, $H_xNO + NO_2 \rightarrow H_{x-1}NO + HONO$ (R12, R16), followed by dissociation of HONO (R6b) to sustain the radical pool. In addition to these major pathways, N_2O is formed in low amounts by NH_2 + NO_2 (R3). Molecular nitrogen is formed from the NH_2 + NO reaction (R4, R5), with its yield controlled to a large extent by the competition between NH_2 + NO (R4, R5) and NH_2 + NO_2 (R2, R3).

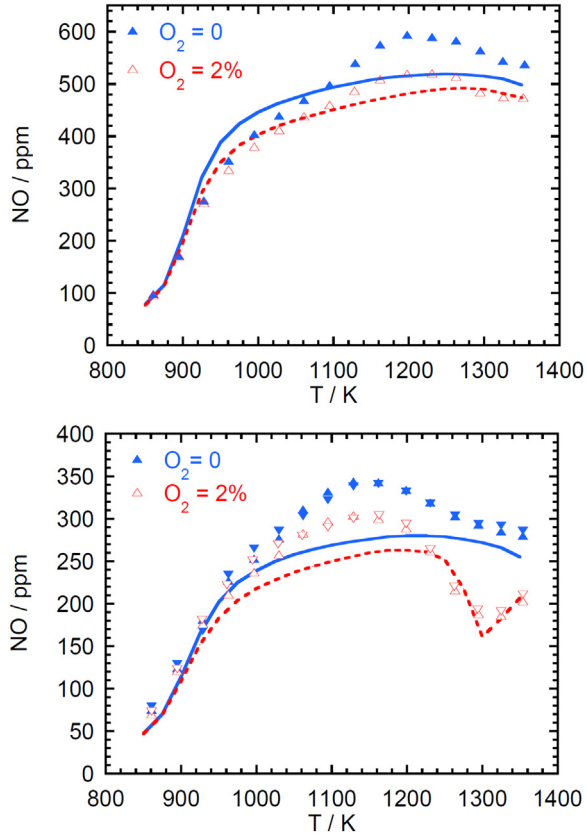

Fig. 8. Comparison of experimental data and modeling predictions for the NO mole fractions in reaction of NH_3/NO_2 mixtures without [19] and with (pw) addition of O_2 in an atmospheric pressure flow reactor. Symbols denote experimental data, while lines denote modeling predictions. Upper figure: NH_3 = 492/483 ppm, NO_2 = 515/505 ppm, NO = 55/55 ppm, O_2 = trace/2.0%. Lower figure: NH_3 = 547/535 ppm, NO_2 = 285/273 ppm, NO = 32/32 ppm, O_2 = trace/2.1%. Carrier gas N_2, residence time (s) ≈ 107/T(K), pressure 1.09 atm. Conditions for repeated experiments are listed in Table 2.

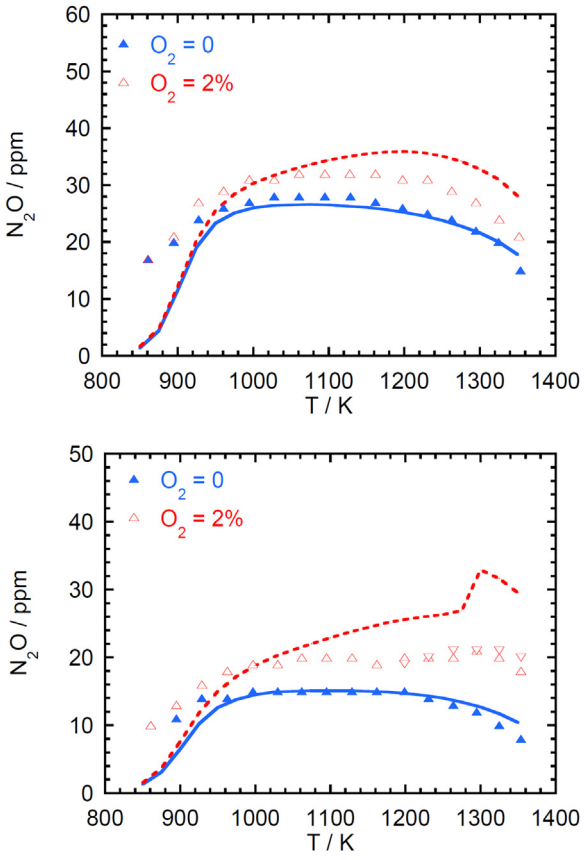

Fig. 9. Comparison of experimental data and modeling predictions for the N_2O mole fractions in reaction of NH_3/NO_2 mixtures without [19] and with (pw) addition of O_2 in an atmospheric pressure flow reactor. Symbols denote experimental data, while lines denote modeling predictions. Upper figure: NH_3 = 492/483 ppm, NO_2 = 515/505 ppm, NO = 55/55 ppm, O_2 = trace/2.0%. Lower figure: NH_3 = 547/535 ppm, NO_2 = 285/273 ppm, NO = 32/32 ppm, O_2 = trace/2.1%. Carrier gas N_2, residence time (s) ≈ 107/T(K), pressure 1.09 atm. Conditions for repeated experiments are listed in Table 2.

Figures 11 and 12 show results for a sensitivity analysis with respect to NO_2 and N_2O, respectively, for the conditions of Figs. 5, 7, and 9. The experimental results and the modeling analysis allow us to constrain the rate parameters for several key reactions in the $NH_3/NO_2/O_2$ reaction system.

The reaction with the largest sensitivity coefficients is that between NH_2 and NO_2 (R2, R3). The present results have implications for both the overall rate constant and the branching fraction. The underprediction of NO above 1100 K indicates that the balance for NH_2 reacting with NO_2 (forming ultimately NO) and NO (leading to N_2) may not be accurate in the present mechanism. Increasing the ratio $(k_2 + k_3) / (k_4 + k_5)$ would yield a better agreement with experiment. While $k(NH_2+NO)$ is well established, the overall rate constant for $NH_2 + NO_2$ is still in discussion and more work on this step at elevated temperatures is desirable.

The measured N_2O profiles, obtained in the absence and presence of O_2, support a branching fraction $\beta = k_3/(k_2 + k_3)$ for the $NH_2 + NO_2$ reaction that decreases with increasing temperature in the 850–1350 K range. The use of a temperature-independent value $\beta = 0.2$, consistent with the measurements of Park and Lin [54,58] (Fig. 3), leads to a significant overprediction of N_2O above 1200 K for all the flow reactor experiments. The temperature dependence observed in the present work is consistent with the interpretation of the NH_3/NO_2 results by Glarborg et al. [19]. It is in good agreement with the theoretical study of Klippenstein et al. [56] and consistent with the low-temperature measurements of Lindholm and Hershberger [59] and Sun et al. [60].

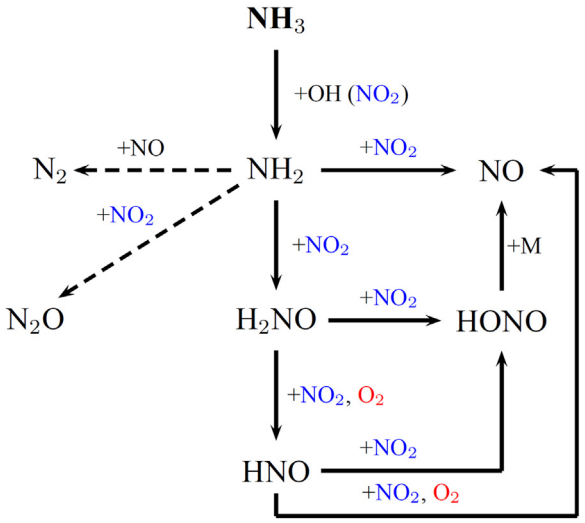

Fig. 10. Pathway diagram for conversion of NH_3 in the presence of NO_2. Additional pathways opening up when O_2 is added are shown in red.

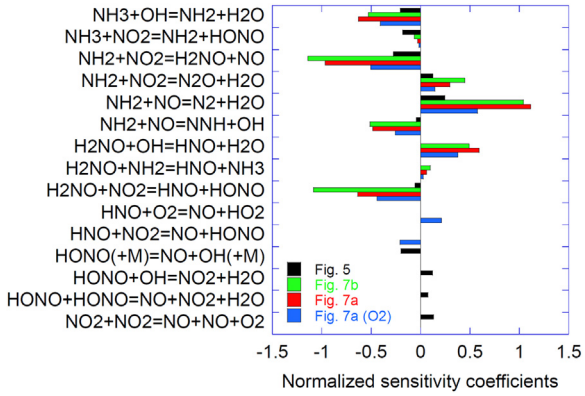

Fig. 11. Sensitivity coefficients for NO_2 for the conditions of Fig. 5 (640 K) and Fig. 7 (1100 K; 285 ppm NO_2 (7b) and 500 ppm NO_2 (7a), wo/w O_2).

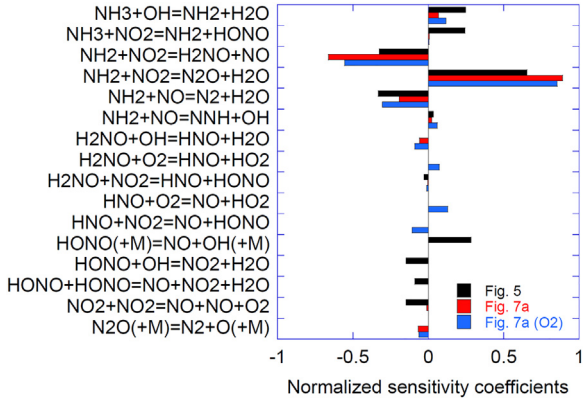

Fig. 12. Sensitivity coefficients for N_2O for the conditions of Fig. 5 (640 K) and Fig. 9a (1250 K; 500 ppm NO_2, wo/w O_2).

The fate of H_2NO and HNO is important for the overall reactivity, both under the present conditions and in ignition of NH_3/air mixtures at engine conditions. As discussed in the Introduction, these oxygenated amines may be involved in chain-branching sequences; either sequence A, $H_2NO + NO_2 \rightarrow HNO + HONO$ (R12), $HNO + NO_2 \rightarrow NO + HONO$ (R16), $HONO (+M) \rightarrow NO + OH (+M)$ (R6b), or sequence B, $NH_2 + NO_2 \rightarrow H_2NO + NO$ (R2), $H_2NO + O_2 \rightarrow HNO + HO_2$ (R10), $HNO + O_2 \rightarrow NO + HO_2$ (R14), $NO + HO_2 \rightarrow NO_2 + OH$ (R17) (the NO_2 recycle sequence). Under the present conditions, sequence A dominates the NH_3/NO_2 experiments, while sequence B becomes important at higher temperatures in the presence of O_2. The satisfactory agreement between experiments and modeling predictions, both without and with O_2, indicates that the rate constants for the reactions of H_2NO and HNO with NO_2 and O_2, respectively, are approximately correct. However, it is a complex reaction system and the constraints on these reactions are dependent on the choice of rate constant for $H_2NO + OH$, for which the theoretical value [17] has not been confirmed experimentally at elevated temperature.

Conclusions

Literature results from batch reactors (580–690 K) [24,25] and flow reactors (850–1350 K) [19] for the NH_3/NO_2 system, supplemented with novel flow reactor results on the impact of O_2 addition, were interpreted in terms of a detailed chemical kinetic model. Batch reactor results on the effect of NO addition on NH_3/NO_2 mixtures allowed a determination of the rate constant for $NH_3 + NO_2$ (R1) at 619 K. The analysis of the flow reactor results indicated that the yield of N_2O in the $NH_2 + NO_2$ reaction (R3) decreases with temperature in the 850–1350 K range, in agreement with the theoretical study by Klippenstein et al. [56]. The flow reactor results for NH_3/NO_2 support a rate constant for $H_2NO + NO_2$ (R12) of approximately $5 \cdot 10^{10}$ cm^3 mol^{-1} s^{-1} at 1000 K. The present analysis also serves to constrain rate constants for the reactions of HNO with NO_2 and O_2, respectively. The findings have implications for modeling ignition and N_2O emissions in ammonia combustion.

Declaration of Competing Interest

The authors declare that they have no known competing financial interests or personal relationships that could have appeared to influence the work reported in this paper.

Acknowledgments

The author would like to thank Jørn Hansen for conducting the experiments and acknowledges support from Innovation Fund Denmark for the AEngine Grand Solutions project and from the European Horizon 2020 program for the Engimmonia project.

Supplementary material

Supplementary material associated with this article can be found, in the online version, at 10.1016/j.combustflame.2022.112311

References

[1] A. Valera-Medina, H. Xiao, M. Owen-Jones, W.I.F. David, P.J. Bowen, Ammonia for power, Prog. Energy Combust. Sci. 69 (2018) 63–102.
[2] H. Kobayashi, A. Hayakawa, K.K.A. Somarathne, E.C. Okafor, Science and technology of ammonia combustion, Proc. Combust. Inst. 37 (2019) 109–133.
[3] A. Valera-Medina, F. Amer-Hatem, A. Azad, I. Dedoussi, M.D. Joannon, R. Fernandes, P. Glarborg, H. Hashemi, X. He, S. Mashurk, J. McGowan, C. Mounaim-Rouselle, A. Ortiz-Prado, J.A. Ortiz-Valera, I. Rossetti, B. Shu, M. Yehia, H. Xiao, M. Costa, A review on ammonia as a potential fuel: from synthesis to economics, Energy Fuels 35 (2021) 6964–7029.
[4] O. Mathieu, E.L. Petersen, Experimental and modeling study on the high-temperature oxidation of ammonia and related NO_x chemistry, Combust. Flame 162 (2015) 554–570.
[5] J. Li, H. Huang, N. Kobayashi, C. Wang, H. Yuan, Numerical study on laminar burning velocity and ignition delay time of ammonia flame with hydrogen addition, Energy 126 (2017) 796–809.
[6] J. Otomo, M. Koshi, T. Mitsumori, H. Iwasaki, K. Yamada, Chemical kinetic modeling of ammonia oxidation with improved reaction mechanism for ammonia/air and ammonia/hydrogen/air combustion, Int. J. Hydrog. Energy 43 (2018) 3004–3014.
[7] P. Glarborg, J.A. Miller, B. Ruscic, S.J. Klippenstein, Modeling nitrogen chemistry in combustion, Prog. Energy Combust. Sci. 67 (2018) 31–68.
[8] B. Mei, X. Zhang, S. Ma, M. Cui, H. Guo, Z. Cao, Y. Li, Experimental and kinetic modeling investigation on the laminar flame propagation of ammonia under oxygen enrichment and elevated pressure conditions, Combust. Flame 210 (2019) 236–246.
[9] B. Mei, J. Zhang, X. Shi, Z. Xi, Y. Li, Enhancement of ammonia combustion with partial fuel cracking strategy: laminar flame propagation and kinetic modeling investigation of $NH_3/H_2/N_2$/air mixtures up to 10 atm, Combust. Flame 231 (2021) 111472.
[10] A. Stagni, C. Cavallotti, S. Arunthanayothin, Y. Song, O. Herbinet, F. Battin-Leclerc, T. Faravelli, An experimental, theoretical and kinetic-modeling study of the gas-phase oxidation of ammonia, React. Chem. Eng. 5 (2020) 696–711.
[11] Y. Jiang, A. Gruber, K. Seshadri, F. Williams, An updated short chemical-kinetic nitrogen mechanism for carbon-free combustion applications, Int. J. Energy Res. 44 (2020) 795–810.
[12] M. Pochet, V. Dias, B. Moreau, F. Foucher, H. Jeanmart, F. Contino, Experimental and numerical study, under LTC conditions, of ammonia ignition delay with and without hydrogen addition, Proc. Combust. Inst. 37 (2019) 621–629.
[13] X. He, B. Shu, D. Nascimento, K. Moshammer, M. Costa, R.X. Fernandes, Auto-ignition kinetics of ammonia and ammonia/hydrogen mixtures at intermediate temperatures and high pressures, Combust. Flame 206 (2019) 189–200.
[14] L. Dai, S. Gersen, P. Glarborg, H. Levinsky, A. Mokhov, Experimental and numerical analysis of the autoignition behavior of NH_3 and NH_3/H_2 mixtures at high pressure, Combust. Flame 215 (2020) 134–144.
[15] Y. Song, H. Hashemi, J. Christensen, C. Zou, P. Marshall, P. Glarborg, Ammonia oxidation at high pressure, Fuel 181 (2016) 358–365.
[16] P. Glarborg, H. Hashemi, S. Cheskis, A.W. Jasper, On the rate constant for $NH_2 + HO_2$ and third-body collision efficiencies for $NH_2 + H$ (+ M) and $NH_2 + NH_2$ (+ M), J. Phys. Chem. A 125 (2021) 1505–1516.

[17] S.J. Klippenstein, P. Glarborg, Theoretical kinetics predictions for NH_2 + HO_2, Combust. Flame 236 (2022) 111787.
[18] J.E.C. Cañas, M. Monge-Palacios, X. Zhang, S.M. Sarathy, Probing the gas-phase oxidation of ammonia: addressing uncertainties with theoretical calculations, Combust. Flame 235 (2022) 111708.
[19] P. Glarborg, K. Dam-Johansen, J.A. Miller, The reaction of ammonia with nitrogen dioxide in a flow reactor: implications for the NH_2+NO_2 reaction, Int. J. Chem. Kinet. 27 (1995) 1207–1220.
[20] J.A. Miller, P. Glarborg, Modeling the formation of N_2O and NO_2 in the thermal De-NO_x process, in: J. Wolfrum, H.-R. Volpp, R. Rannacher, J. Warnatz (Eds.), Gas-phase Chemical Reaction Systems: Experiments and Modeling 100 Years after Max Bodenstein, Springer Series in Chemical Physics 61 (1996), pp. 318–333.
[21] J.A. Miller, P. Glarborg, Modeling the thermal DeNO_x process: closing in on a final solution, Int. J. Chem. Kinet. 31 (1999) 757–765.
[22] S. Klippenstein, L. Harding, P. Glarborg, J. Miller, The role of NNH in NO formation and control, Combust. Flame 158 (2011) 774–789.
[23] W.A. Rosser Jr, H. Wise, Gas-phase oxidation of ammonia by nitrogen dioxide, J. Chem. Phys. 25 (1956) 1078–1079.
[24] G. Bedford, J.H. Thomas, Reaction between ammonia and nitrogen dioxide, J. Chem. Soc. Faraday Trans. 1 68 (1972) 2163–2170.
[25] J. Park, S. Gates, M.-C. Lin, Photolytically and thermally initiated reactions of NH_3 with NO_x (x = 1, 2), Combust. Sci. Technol. 182 (2010) 365–379.
[26] P.G. Kristensen, P. Glarborg, K. Dam-Johansen, Nitrogen chemistry during burnout in fuel-staged combustion, Combust. Flame 107 (1996) 211–222.
[27] M.P. Burke, M. Chaos, Y. Ju, F.L. Dryer, S.J. Klippenstein, Comprehensive H_2/O_2 kinetic model for high-pressure combustion, Int. J. Chem. Kinet. 44 (2012) 444–474.
[28] H. Hashemi, J.M. Christensen, S. Gersen, P. Glarborg, Hydrogen oxidation at high pressure and intermediate temperatures: experiments and kinetic modeling, Proc. Combust. Inst. 35 (2015) 553–560.
[29] M.P. Burke, S.J. Klippenstein, Ephemeral collision complexes mediate chemically termolecular transformations that affect system chemistry, Nat. Chem. 9 (2017) 1078–1082.
[30] S.J. Klippenstein, R. Sivaramakrishnan, U. Burke, K.P. Somers, H.J. Curran, L. Cai, H. Pitsch, M. Pelucchi, T. Faravelli, P. Glarborg, HO_2 + HO_2: High level theory and the role of singlet channels, Combust. Flame 2022 (2022), doi:10.1016/j.combustflame.2021.111975.
[31] P. Glarborg, H. Hashemi, P. Marshall, Challenges in kinetic modeling of ammonia pyrolysis, Fuel Commun. 10 (2022) 100049.
[32] P. Marshall, G. Rawling, P. Glarborg, New reactions of diazene and related species for modelling combustion of amine fuels, Mol. Phys. 119 (2021) e1979674.
[33] S. Song, R.K. Hanson, C.T. Bowman, D.M. Golden, Shock tube determination of the overall rate of NH_2 + NO → products in the thermal De-NO_x temperature window, Int. J. Chem. Kinet. 33 (2001) 715–721.
[34] D. Fulle, H.F. Hamann, H. Hippler, J. Troe, Temperature and pressure dependence of the addition reactions of HO to NO and to NO_2. IV. Saturated laser-induced fluorescence measurements up to 1400 bar, J. Chem. Phys. 108 (1998) 5391–5397.
[35] J.B. Burkholder, A. Mellouki, R. Talukdar, A.R. Ravishankara, Rate coefficients for the reaction of OH with HONO between 298 and 373 K, Int. J. Chem. Kinet. 24 (1992) 711–725.
[36] M. Page, M.R. Soto, Radical addition to HNO. *ab initio* reaction path and variational transition state theory calculations for H + HNO → H_2NO and H + HNO → HNOH, J. Chem. Phys. 99 (1993) 7709–7717.
[37] A.M. Dean, J.W. Bozzelli, Combustion chemistry of nitrogen, in: W. Gardiner (Ed.), Gas phase combustion chemistry, Springer-Verlag, 2000.
[38] W. Tsang, J.T. Herron, Chemical kinetic data base for propellant combustion I. Reactions involving NO, NO_2, HNO, HNO_2, HCN and N_2O, J. Phys. Chem. Ref. Data 20 (1991) 609–663.
[39] P.S. Riley, B. Cosic, A. Fontijn, The H + NO recombination reaction over a wide temperature range, Int. J. Chem. Kinet. 35 (2003) 374–380.
[40] Q.-D. Wang, Y. Sun, H.J. Curran, Comparative chemical kinetic analysis and skeletal mechanism generation for syngas combustion with No_x chemistry, Energy Fuels 34 (2019) 949–964.
[41] S. Xu, M.-C. Lin, Ab initio chemical kinetics for the NH_2 + HNO_x reactions, part i: kinetics and mechanism for NH_2 + HNO, Int. J. Chem. Kinet. 41 (2009) 667–677.
[42] Y. Shang, J. Shi, H. Ning, R. Zhang, H. Wang, S. Luo, Ignition delay time measurements and kinetic modeling of CH_4 initiated by CH_3NO_2, Fuel 243 (2019) 288–297.
[43] D.L. Baulch, C.T. Bowman, C.J. Cobos, R.A. Cox, T. Just, J.A. Kerr, M.J. Pilling, D. Stocker, J. Troe, W. Tsang, R.W. Walker, J. Warnatz, Evaluated kinetic data for combustion modeling: supplement II, J. Phys. Chem. Ref. Data 34 (2005) 757–1397.
[44] S. Xu, M.-C. Lin, Ab initio chemical kinetics for the NH_2 + HNO_x reactions, part II: kinetics and mechanism for NH_2 + HONO, Int. J. Chem. Kinet. 41 (2009) 678–688.
[45] A.G. Thaxton, C.-C. Hsu, M.-C. Lin, Rate constant for the NH_3 + NO_2→ NH_2 + HONO reaction: comparison of kinetically modeled and predicted results, Int. J. Chem. Kinet. 29 (1997) 245–251.
[46] A.M. Mebel, E.W.G. Diau, M.-C. Lin, K. Morokuma, Theoretical rate constants for the NH_3 + NO_x→ NH_2 + HNO_x (x = 1, 2): reactions by ab initio MO/VTST Calculations, J. Phys. Chem. 100 (1996) 7517–7525.
[47] W. Hack, H. Schacke, M. Schröter, H.G. Wagner, Reaction rates of NH_2-radicals with NO, NO_2, C_2H_2, C_2H_4 and other hydrocarbons, Symp. (Int.) Combust. 17 (1979) 505–513.
[48] H. Kurasawa, R. Lesclaux, Kinetics of the reaction of NH_2 with NO_2, Chem. Phys. Lett. 66 (1979) 602–607.
[49] A.R. Whyte, L.F. Phillips, Rates of reactions of NH_2 with NO and NO_2, Chem. Phys. Lett. 102 (1983) 451–454.
[50] T.X. Xiang, L.M. Torres, W.A. Guillory, State-selected reaction and relaxation of NH_2 radicals and NO_2, J. Chem. Phys. 83 (1985) 1623–1629.
[51] V.P. Bulatov, A.A. Ioffe, V.A. Lozovsky, O.M. Sarkisov, On the reaction of the NH_2 radical with NO_2 at 295-620 Kk, Chem. Phys. Lett. 159 (1989) 171–174.
[52] P. Pagsberg, B. Sztuba, E. Ratajczak, A. Sillesen, Spectrokinetic studies of the gas-phase reactions NH_2 + NO_x initiated by pulse-radiolysis, Acta Chem. Scand. 45 (1991) 329–334.
[53] H. Meunier, P. Pagsberg, A. Sillesen, Kinetics and branching ratios of the reactions NH_2 + NO_2→ N_2O + H_2O and NH_2 + NO_2→ H_2NO + NO studied by pulse radiolysis combined with time-resolved infrared diode laser spectroscopy, Chem. Phys. Lett. 261 (1996) 277–282.
[54] J. Park, M.C. Lin, A mass spectrometric study of the NH_2 + NO_2 reaction, J. Phys. Chem. A 101 (1997) 2643–2647.
[55] S. Song, D.M. Golden, R.K. Hanson, C.T. Bowman, A shock tube study of the NH_2 + NO_2 reaction, Proc. Combust. Inst. 29 (2002) 2163–2170.
[56] S.J. Klippenstein, L.B. Harding, P. Glarborg, Y. Gao, P. Marshall, Rate constant and branching fraction for the NH_2 + NO_2 reaction, J. Phys. Chem. A 117 (2013) 9011–9022.
[57] R.W. Quandt, J.F. Hershberger, Diode laser study of the product branching ratio of the NH_2 + NO_2 reaction, J. Phys. Chem. 100 (1996) 9407–9411.
[58] J. Park, M.C. Lin, Mass-spectrometric determination of product branching probabilities for the NH_2 + NO_2 reaction at temperatures between 300 and 990 K, Int. J. Chem. Kinet. 28 (1996) 879–883.
[59] N. Lindholm, J.F. Hershberger, Product branching ratios of the NH_2 + NO_2 reaction, J. Chem. Phys. A 101 (1997) 4991–4995.
[60] F. Sun, J.D. DeSain, G. Scott, P.Y. Hung, R.I. Thompson, G.P. Glass, R.F. Curl, Reactions of NH_2 with NO_2 and of OH with NH_2O, J. Phys. Chem. A 105 (2001) 6121–6128.
[61] J. Cui, S. Zhao, X. Liu, L. Yang, S. Sun, J. Zhang, Theoretical studies on NH_2 + NO_2 reaction: driven by reaction dynamics, Int. J. Mass Spectrom. 462 (2021) 116522.
[62] X. Chen, M.E. Fuller, C.F. Goldsmith, Decomposition kinetics for HONO and HNO_2, React. Chem. Eng. 4 (2019) 323–333.
[63] C.J. Howard, K.M. Evenson, Laser magnetic resonance study of the gas phase reactions of OH with CO, NO, and NO_2, J. Chem. Phys. 61 (1974) 1943–1952.
[64] J.G. Anderson, J.J. Margitan, F. Kaufman, Gas phase recombination of OH with NO and NO_2, J. Chem. Phys. 60 (1974) 3310–3317.
[65] G.W. Harris, R.P. Wayne, Reaction of hydroxyl radicals with NO, NO_2 and SO_2, J. Chem. Soc. Faraday Trans. 1 71 (1975) 610–617.
[66] R. Atkinson, D.A. Hansen, J.N. Pitts Jr, Rate constants for the reaction of the OH radical with H_2 and NO (M = Ar and N_2), J. Chem. Phys. 62 (1975) 3284–3288.
[67] P. Sharkey, I.R. Sims, I.W.M. Smith, P. Bocherel, B.R. Rowe, Pressure and temperature dependence of the rate constants for the association reaction of OH radicals with NO between 301 and 23 K, J. Chem. Soc. Faraday Trans. 90 (1994) 3609–3616.
[68] R.A. Fifer, Kinetics of the reaction OH + HONO → H_2O + NO_2 at high temperatures behind shock, J. Phys. Chem. 80 (1976) 2717–2723.
[69] A.M. Mebel, M.-C. Lin, K. Morokuma, *Ab initio* MO and TST calculations for the rate constant of the HNO + NO_2→ HONO + NO reaction, Int. J. Chem. Kinet. 30 (1998) 729–736.
[70] J.E. Chavario Cañas, M. Monge-Palacios, X. Zhang, S.M. Sarathy, Probing the gas-phase oxidation of ammonia: addressing uncertainties with theoretical calculations, Combust. Flame 235 (2022) 111708.
[71] M.T. Allen, R.A. Yetter, F.L. Dryer, Hydrogen/nitrous oxide kinetics - Implications of the N_xH_y species, Combust. Flame 112 (1998) 302–311.
[72] P. Glarborg, M. Østberg, M.U. Alzueta, K. Dam-Johansen, J.A. Miller, The recombination of hydrogen atoms with nitric oxide at high temperatures, Symp. (Int.) Combust. 27 (1998) 219–226.
[73] A.M. Dean, J.E. Hardy, R.K. Lyon, Kinetics and mechanism of NH_3 oxidation, Symp. (Int.) Combust. 19 (1982) 97–105.
[74] R.A. Yetter, F.L. Dryer, H. Rabitz, Flow reactor studies of carbon monoxide/hydrogen/ oxygen kinetics, Combust. Sci. Technol. 79 (1991) 129–140.